Journal of Marine Science and Application (2026) 25: 277-291
https://doi.org/10.1007/s11804-025-00690-9

RESEARCH ARTICLE

Influence of Geometric Parameters of Pre-Chamber on Mixture Formation in Marine Ammonia/Hydrogen Engines

Shuzhe Yan[1], Shengli Wei[1], Yuhao Lu[1], Yuanchen Li[1] and Yuhan Li[1]

Received: 28 October 2024 / Accepted: 10 February 2025

Abstract

Pre-chamber ignition technology can address the issue of uneven in-cylinder mixture combustion in large-bore marine engines. The impact of various pre-chamber structures on the formation of the mixture and jet flames within the pre-chamber is explored. This study performed numerical simulations on a large-bore marine ammonia/hydrogen pre-chamber engine prototype, considering pre-chamber volume, throat diameter, the distance between the hydrogen injector and the spark plug, and the hydrogen injector angle. Compared with the original engine, when the pre-chamber volume is 73.4 ml, the throat diameter is 14 mm, the distance ratio is 0.92, and the hydrogen injector angle is 80°. Moreover, the peak pressure in the pre-chamber increased by 23.1%, and that in the main chamber increased by 46.3%. The results indicate that the performance of the original engine is greatly enhanced by altering its fuel and pre-chamber structure.

Keywords Pre-chamber ignition; Ammonia/hydrogen fuel; Pre-chamber mixture formation; Jet characteristics; Marine engine

1 Introduction

The transportation industry faces an increasing demand for sustainable energy solutions as environmental concerns and stricter greenhouse gas emission regulations continue to rise. The reliance on fossil fuels has not only accelerated climate change but also intensified air pollution; thus, new regulatory frameworks have been adopted (Haruna et al., 2023). For example, the International Maritime Organization (IMO) introduced the "2023 IMO GHG Strategy" to enforce stricter controls on emissions from the maritime sector. Consequently, engine manufacturers explore alternative fuels and new combustion technologies to satisfy these stringent targets (Kleeman et al., 2013).

One promising approach is the use of low- or zero-carbon fuels, such as hydrogen, ammonia, and natural gas, which can significantly reduce carbon emissions from ships. Coupling these fuels with advanced technologies, such as pre-chamber ignition (PCI), lean burn combustion, and exhaust gas recirculation, can further enhance fuel efficiency while minimizing pollutant emissions (Bunce et al., 2014).

PCI is particularly effective as it facilitates lean burn combustion by reducing in-cylinder temperatures, thereby minimizing fuel consumption and the emission of pollutants (such as NO_x) (Dale and Oppenheim, 1981; Zhu et al., 2022). The high ignition energy and rapid flame propagation provided by PCI improve combustion efficiency and stability, which is especially critical in large-bore marine engines.

Ammonia has received considerable attention as a carbon-free fuel with high potential for marine applications due to its high octane rating and excellent resistance to knocking.

However, the relatively low chemical reactivity of ammonia presents a challenge in terms of ignition in internal combustion engines. Ammonia is combined with hydrogen, a highly reactive fuel, to enhance the combustion process, overcoming this limitation. Hydrogen can significantly improve flame propagation and ensure stable combustion, especially under lean conditions. The generated hot jet enhances ammonia combustion and flame propagation by using a hydrogen jet to ignite ammonia in the main chamber (MC), ensuring stable combustion at low-equivalence ratios (Liu et al., 2023a). This method is particularly impor-

Article Highlights

- Pre-chamber ignition system can improve marine engine combustion performance.
- A pre-chamber structure that is conducive to the formation of mixture and jet flame.
- A new dimensionless number-distancing ratio-is defined.
- The first peak pressure in the pre-chamber increased by 23.1%.
- The peak pressure in the main chamber increased by 46.3%.

✉ Shengli Wei
weishengli@ujs.edu.cn

[1] School of Automotive and Traffic Engineering, Jiangsu University, Zhenjiang 212013, China

tant in large-bore engines, where slow combustion can be problematic. Moreover, hydrogen combustion produces only water as a byproduct, rendering it environmentally friendly for reducing greenhouse gas emissions (Liu et al., 2022).

The active PCIs can markedly increase engine efficiency and the limits of lean burn (Attard et al., 2010). A large amount of CO and HC is generated upon ignition of the mixture in the pre-chamber (PC) (Jamrozik, 2015). The hot combustion products are injected into the cylinder through the nozzles and rapidly burn in the MC as the pressure in the PC rises. The jet flame reduces the sensitivity of heat release to variations in the equivalence ratio, simplifying the combustion control strategies and partially suppressing knock (Wu et al., 2018). The addition of hydrogen as an auxiliary fuel in the PC can enhance the lean burn limit, mixture reactivity, initial flame kernel volume, and combustion rate in the MC (Sun et al., 2022; Liu et al., 2023b). Compared with traditional ignition systems, hydrogen-based active ignition systems increase combustion stability and mean effective pressure and decrease the indicated fuel consumption rate (Liu and Zhou, 2023).

The PC volume, throat diameter, and spark plug position influence the development of the jet flame, exhibiting the combustion characteristics of the MC. A PC with lower heat transfer losses and smaller volume exhibits enhanced overall indicated efficiency and fuel economy. Increasing the PC volume results in faster jet velocities, intensifying turbulence and heat transfer losses in the MC (Hlaing et al., 2022). The spark plug position significantly affects ignition delay and turbulence generation (Biswas and Qiao, 2018). Igniting near the nozzle ensures complete combustion of the mixture in the PC, minimizing unburned fuel leakage into the MC. The hot products formed enter the MC at a more consistent injection speed and with an extended injection duration, strengthening combustion in the MC (Validi et al., 2017). When the spark plug is positioned further from the nozzle, the ignition delay is increased.

For marine large-bore engines, combining ammonia/hydrogen with PCI technology can enhance the combustion speed of the in-cylinder mixture and reduce pollutant emissions. The mixture formation in the PC influences the jet flame characteristics, subsequently affecting the combustion and emissions in the MC.

This study focuses on the application of PCI technology in a marine ammonia/hydrogen engine, investigating various design parameters of the PC and their influence on combustion performance. The research uses numerical simulations to evaluate key factors, such as PC volume, throat diameter, the distance between the hydrogen injector and spark plug, and the hydrogen injector angle. The equivalence ratio of the mixture in the PC is compared with the temperature fields of the PC and MC, providing insights for improving fuel efficiency and reducing emissions in large-bore marine engines.

2 Experimental setup

2.1 Model and mesh

The combustion system for the proposed large-bore marine ammonia/hydrogen jet ignition engine is illustrated in Figure 1. A premixed ammonia/hydrogen gas mixture, with an equivalence ratio of 0.5, is introduced into the MC. Hydrogen is injected into the PC through an injector, with an equivalence ratio of 1, and ignited using a spark plug. This ignition generates a jet flame, which then enters the MC through the jet orifice, subsequently igniting the mixture present in the MC.

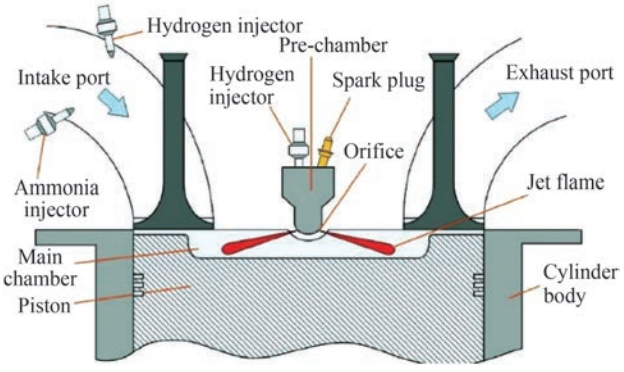

Figure 1 Ammonia/hydrogen jet ignition engine combustion system

This study uses the 6ACD320G high-power marine medium-speed natural gas engine as the baseline model. The fuel nozzle in the PC was replaced with a hydrogen injector, converting it into an active PC jet ignition system for this investigation. Table 1 shows the main parameters. To simulate the flow dynamics, spray behavior, and combustion processes within the engine's working cycle, 3D CFD software, CONVERGE v3.0, was employed.

Table 1 Main parameters of the 6ACD320G engine with pre-chamber

Type	6-cylinder, 4-stroke
Bore (mm)	320
Stroke (mm)	420
Connecting rod length (mm)	920
Compression ratio	12.5
Engine power (kW)	2430
Engine speed (r/min)	750

Figure 2 illustrates the geometric model of the PCI engine, including intake ports, exhaust ports, MC, and PC. An ammonia/hydrogen fuel injector is placed in the intake port, and a hydrogen injector is positioned above the PC. The PC is initially sized to 2.0% of the engine's clearance volume. Eight orifices, each with a diameter of 3 mm, are positioned at the base of the PC and connected to the MC.

The jet direction forms a 70° angle relative to the central axis of the PC.

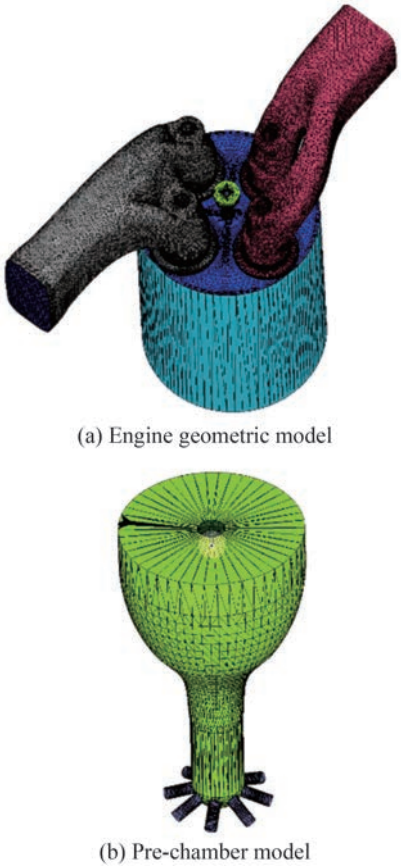

(a) Engine geometric model

(b) Pre-chamber model

Figure 2 Engine's 3D geometric model

The RNG $k-\varepsilon$ turbulence model was applied to capture the in-cylinder flow dynamics, covering a broad range of Reynolds numbers and providing accurate predictions of in-cylinder turbulence intensity. The SAGE detailed chemical kinetics solver was applied to compute the combustion reactions of the ammonia/hydrogen mixture, using reaction mechanisms compatible with CHEMKIN format files. The hydrogen/ammonia chemical reaction mechanism improved by Yu et al. (2024) is adopted; it comprises 34 species and 286 reaction steps.

2.2 Initial and boundary conditions

The geometric model developed for this study was integrated into the CONVERGE software, where the in-cylinder combustion process was simulated under operating conditions of 750 r/min and 27.8 kN·m of torque. In this simulation, the 360° crank angle (CA) corresponds to TDC. The simulation begins at 300° CA when the exhaust valve from the previous cycle opens and concludes at 1 020° CA after the exhaust valve of the current cycle closes. This setup models one complete engine cycle. The initial and boundary conditions for the simulation are detailed in Table 2.

Table 2 Initial and boundary conditions

Conditions	Region	Temperature (K)	Pressure (MPa)
Initial	Intake port	318	0.35
	Exhaust port	1 000	0.35
	Pre-chamber	1 200	0.39
	Main chamber	1 200	0.39
Boundary	Intake valve	318	0.35
	Exhaust valve	1 000	0.35
	Pre-chamber wall	700	–
	Cylinder head bottom	623	–
	Cylinder liner wall	520	–
	Piston top surface	620	–

2.3 Model verification

A grid independence verification was conducted to determine a suitable base mesh size. Calculations were performed using four base mesh sizes: 8.0, 9.0, 10.0, and 11.0 mm. The average in-cylinder temperature and pressure of the MC, illustrated in Figure 3, were evaluated. When the base mesh size was reduced to 10.0 mm, the key parameters demonstrated convergence. Consequently, a 10.0 mm base mesh size was selected for the simulation, with additional local mesh refinement applied as required.

As shown in Figure 4, the calculated curves corresponded with the experimental data during the compression and com-

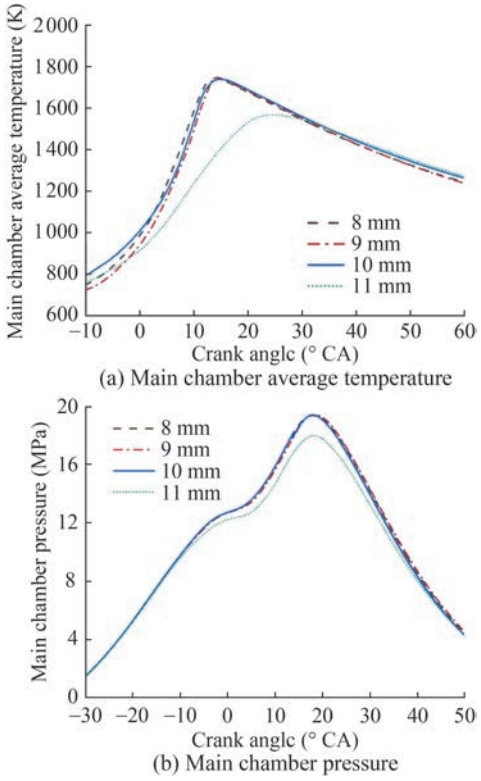

Figure 3 Simulation results of different basic grid sizes

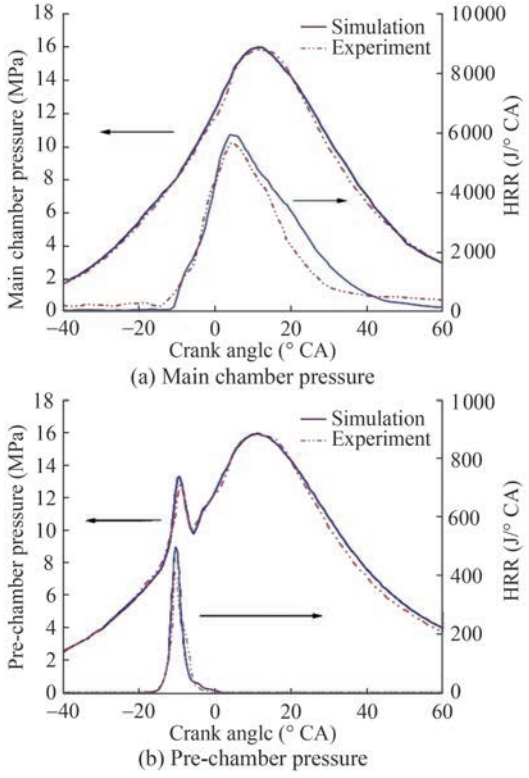

Figure 4 Comparison of experimental and calculated in-cylinder pressures and HRR

bustion stages, with the peak phases of pressure and heat release rate (HRR) being approximately the same and an error of less than 3%. This finding satisfies the requirements for simulation calculations.

2.4 Calculation case

Latsch and Schlembach (1980) suggested that the optimal range for the PC volume is 1%–4% of the clearance volume. This study considered cases with PC volumes of 2.0%, 2.5%, 3.0%, 4.0%, and 5.0% of the clearance volume. The throat diameter of the PC is usually determined using the dimensionless parameter C_t, which represents the degree of fuel mixing within the PC and is defined as follows:

$$C_t = \left[\left(\frac{D}{d}\right)^2 - \frac{1}{2}\right]^{-\frac{1}{2}} \quad (1)$$

where D denotes the inner diameter of the PC, whereas d represents the throat diameter. Anderson et al. (1984) indicated that the optimal range for the Craya–Curtet number is 0.2 to 0.3. This study selected C_t values of 0.18, 0.22, 0.24, 0.26, 0.28, and 0.32 as cases, with corresponding PC throat diameters of 9, 11, 12, 13, 14, and 16 mm, respectively. The distances between the hydrogen injector and spark plug within the PC were set at 16, 19, 21.5, 23.5, and 24.5 mm. The orientation of the hydrogen injector was defined such that it faced directly toward the spark plug at 0°, whereas that facing toward the PC wall corresponded to 90°. To facilitate effective mixture formation through the intake airflow field development in the PC design, various angles of 50°, 60°, 70°, 80°, and 90° were considered.

3 Results and discussion

3.1 Volume of pre-chamber

Subtle modifications in the PC design can greatly influence the performance of the PCI. The PC volume plays a crucial role in determining the amount of energy generated during mixture combustion. A larger PC requires more fuel to generate energy and, under the same conditions, produces higher jet energy. At higher ignition energies, this condition results in turbulent jets impacting the walls of the MC. However, an excessively large PC volume increases heat dissipation losses, reduces the overall engine compression ratio, and theoretically minimizes thermal efficiency. Conversely, a smaller PC requires less fuel, can achieve stable combustion, and maintains higher system efficiency.

Thus, to explore the impact of PC volume, five cases with PC volumes of 58.8, 73.4, 88.1, 117.5, and 146.9 ml were used. For convenience of analysis, these cases are labeled as V-2, V-2.5, V-3, V-4, and V-5. Except for the PC volume, all other structural parameters remain unchanged.

3.1.1 Formation of the pre-chamber mixture

In this study, the moment when the piston reaches TDC during the compression stroke is designated as 0° CA. Figure 5 illustrates the equivalence ratio distribution in the PC from the end of hydrogen injection (−105° CA aTDC) to the ignition timing (−16° CA aTDC).

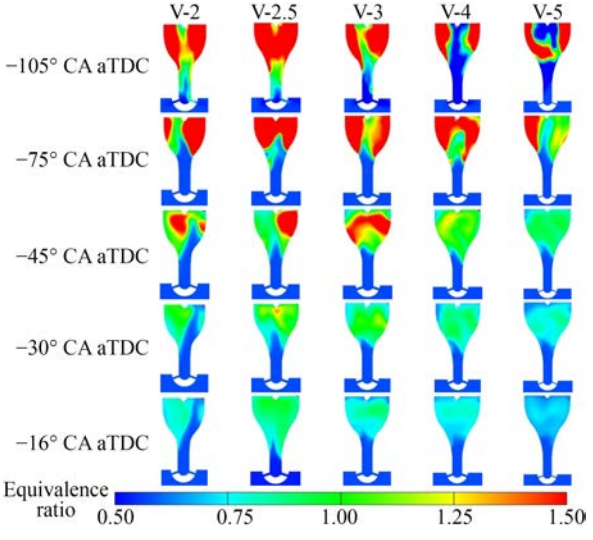

Figure 5 Equivalence ratio of the PC at different volumes and at different times

Upon the completion of hydrogen injection, an increase in PC volume leads to pronounced overly rich or overly lean mixture conditions, particularly in V-4 and V-5. This phenomenon occurs because, while the quantity of hydrogen injected remains constant, expanding the PC volume reduces the flow velocity of the mixture inside the PC.

With a smaller PC volume, richer mixtures form near the spark plug in V-2, V-2.5, and V-3. As the PC volume increases, the mixture concentration near the spark plug decreases in V-4 and V-5. When the PC volume becomes excessively large, the tumble angular momentum of the mixture decreases, reducing the turbulence intensity in the PC at the end of hydrogen injection. Increasing the PC volume decreases the overly rich regions of the mixture inside the PC, aiding in the rapid formation of a uniform mixture. The most notable changes occur in V-5, where, by 29° CA prior to ignition, no overly rich mixture remains inside the PC.

At the ignition phase, none of the five PC volume cases show overly rich mixture conditions. However, a concentrated mixture distribution located opposite the hydrogen injector is observed in V-2, causing the overall mixture distribution in PC to be uneven. In V-4 and V-5, the equivalence ratio in PC has already become extremely low. As the PC volume is increased, the lean mixture from the MC occupies a greater proportion of the PC, resulting in a leaner overall mixture. This condition is detrimental to the ignition of the mixture and the ensuing propagation of the jet flame. The comparison between V-2.5 and V-3 evidently shows that the mixture distribution in V-2.5 is broader and more uniform, with an equivalence ratio of approximately 1, consistent with expectations.

3.1.2 Distribution of the temperature field

The quality of mixture formation in the PC directly affects the mixture combustion, and the formation of jet flame further impacts the MC combustion. This section provides a comparative analysis of the temperature fields in the PC and MC. Figure 6 illustrates the combustion temperature distribution cloud charts in the PC and MC for different PC volumes. Starting from the end of ignition timing (−14° CA aTDC) to 4° CA aTDC. Each set of cloud charts is divided into upper and lower views, with the upper view illustrating a sectional view on the *zx* plane and the lower view demonstrating an axial sectional view 10 mm below the intake and exhaust port horizontal plane.

When the mixture in the PC is ignited using the spark plug, a jet flame is formed and shoots into the MC through the connecting orifices between the PC and the MC. In V-2, V-2.5, and V-3, jet flames are already generated at −12° CA aTDC. Additionally, the jet flame generated in V-2.5 is longer and has a larger area. As the PC volume increases, it enhances ignition energy, speeds up flame propagation, and extends injection duration. At −8° CA aTDC, the flames from the PC in all cases had entered the MC and initiated combustion. With increasing PC volume, the flame front area in the MC initially expands but then contracts.

In the V-2.5 case, the flame front area in the MC reaches its peak, leading to more thorough combustion. As the PC volume increases further, the flame front area shrinks, flame

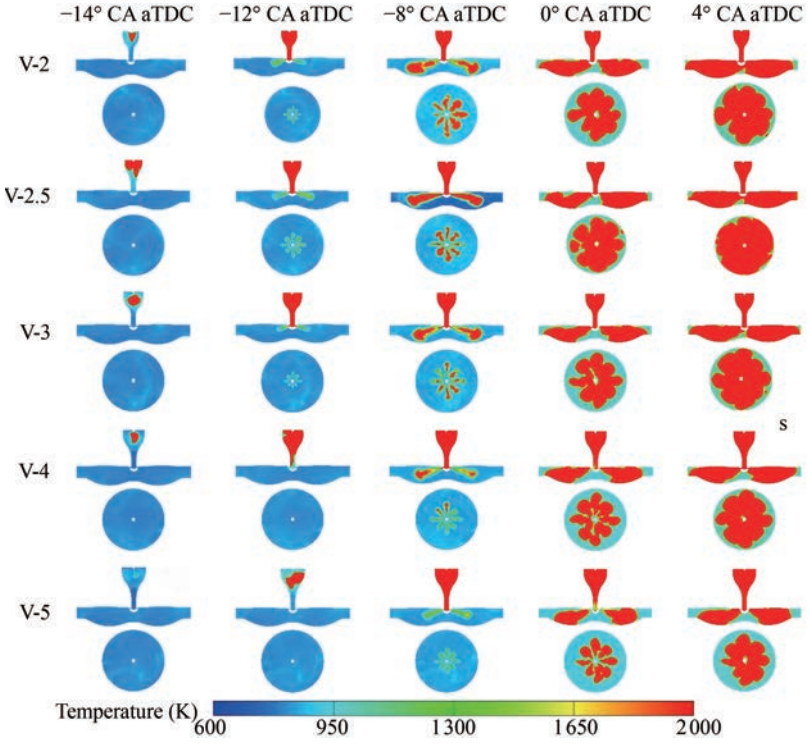

Figure 6 Temperature distribution cloud diagram of the PC and the MC

propagation slows, and the overall combustion rate declines. As the PC volume continuously increases, although the mixture in the PC increases, excessive lean mixture from the MC is compressed into the PC. The mixture in the PC becomes leaner, reducing the jet flame energy and the flame front area in the MC.

3.1.3 Combustion properties

Figure 7 illustrates that the pressure curve in the PC exhibits two distinct peaks. The first peak appears at the ignition moment when the spark plug ignites the fuel mixture within the PC. Following ignition, high-temperature combustion products are generated and expelled into the MC through the PC orifices, initiating combustion in the MC. The second peak arises after TDC when the jet from the PC has mostly concluded. Among the cases, V-2 exhibits the highest first peak pressure, reaching 16.9 MPa, whereas the second peak pressures for V-2.5 and V-3 are 16.1 and 16.2 MPa, respectively. The first peak pressures in the PC for these cases demonstrate minimal variation and are higher than those recorded in V-4 and V-5. In V-2.5, the fuel mixture in the PC is more evenly distributed, resulting in earlier ignition and an earlier peak pressure. Increasing the PC volume allows more fuel to participate in combustion, thereby producing a higher HRR. However, as the volume increases, the mixture uniformity decreases, leading to a significant combustion delay. The timing of the peak HRR in V-5 lags by 2.6° CA compared with V-2.5.

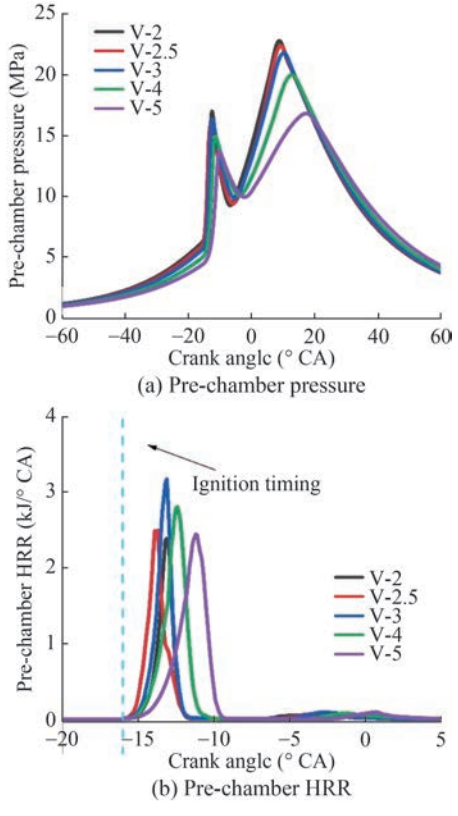

Figure 7 PC pressure and HRR curves under different PC volumes

To further characterize the jet characteristics of the PC, the max pressure difference between the PC and the MC is defined as the max PC pressure difference. As shown in Figure 8, the max pressure differences for V-2, V-2.5, and V-3 are 9.0, 8.8, and 8.9 MPa, respectively, which are all higher than those for V-4 and V-5. In the first three cases, the equivalence ratio of the mixture within the PC is nearly 1, whereas in V-4 and V-5, the equivalence ratio drops to below 1, indicating a leaner mixture. A leaner mixture in the PC reduces the max pressure difference, which consequently minimizes the jet velocity and slows flame propagation. For V-2.5, the max pressure difference occurs at −12.8° CA, which is the closest to the ignition timing among the five cases, suggesting that the jet from the PC initiates earlier in this scenario.

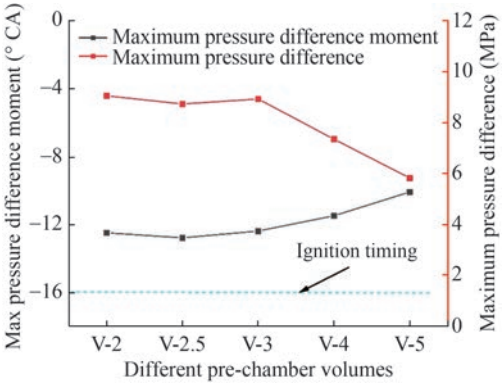

Figure 8 Pre-chamber pressure difference and maximum pressure difference moment

Figure 9 presents the pressure and HRR curves for the MC. The peak pressure in case V-2.5 reaches the highest value of 23.1 MPa, occurring at 6.9° CA aTDC. It is followed by V-2, V-3, V-4, and V-5, with peak pressures of 22.9, 22.8, 21.9, and 17.3 MPa, respectively, occurring at 7.3° CA, 7.3° CA, 8.7° CA, and 14.1° CA aTDC. The peak HRR values for V-2.5, V-2, and V-4 are nearly identical. However, V-2.5 has the most homogeneous mixture in the PC, and the jet appears earlier than in the other cases. The MC in V-2.5 begins combustion the earliest, whereas in the four other cases, it exhibits varying degrees of combustion delay.

3.2 Throat diameter of pre-chamber

Variations in the throat diameter of the PC influence the mass exchange between the mixture in the MC and the PC. In this study, the throat diameter of the PC was varied while maintaining constant PC volume and height. According to the definition of the C_t number, six different throat diameters were selected for analysis: 9, 11, 12, 13, 14, and 16 mm.

3.2.1 PC mixture formation

Figure 10 illustrates the distribution of the equivalence

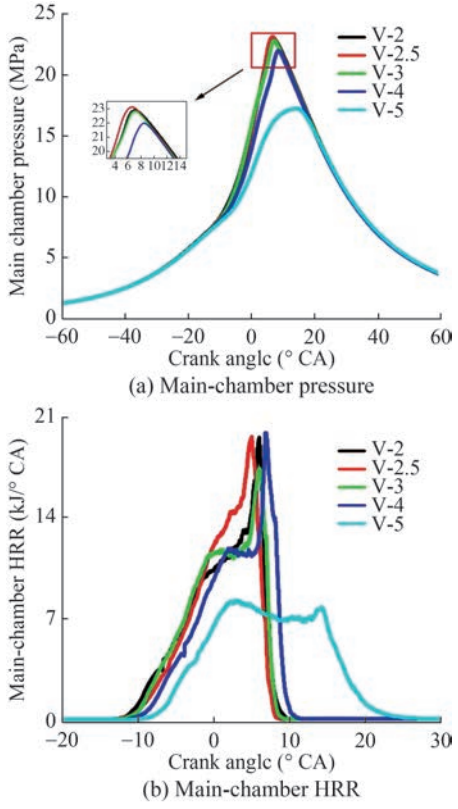

Figure 9 MC pressure and HRR curves under different PC volumes

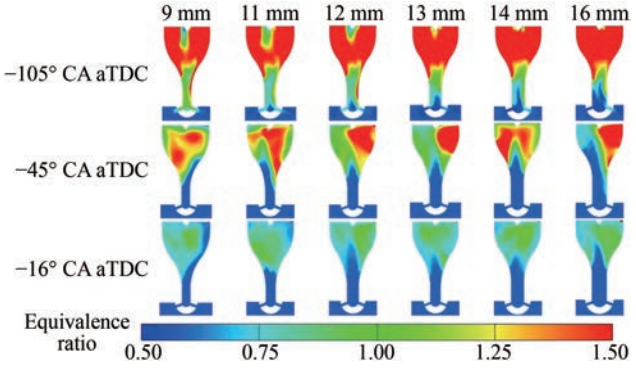

Figure 10 Equivalence ratio distribution in the PC under different throat diameters

ratio within the PC at various time points for different throat diameters. At the end of hydrogen injection, PCs with throat diameters of 9, 11, and 12 mm demonstrate an uneven equivalence ratio distribution near the spark plug. Given that the overall height and volume of the PC remain constant, reducing the throat diameter decreases the volume in the lower throat region and increases the volume in the upper section, effectively broadening the PC.

The mixture cannot flow adequately, leading to locally overly lean areas in the equivalence ratio distribution. At ignition timing, the PCs with 9 and 11 mm throat diameters still present locally overly lean mixtures. As the piston moves upward, the low-equivalence ratio mixture entering the PC from the MC cannot mix in time. This condition indicates that an extremely small PC throat diameter is not conducive to mixture formation. PCs with throat diameters of 12, 13, and 14 mm form mixtures with an equivalence ratio of 1, with the 13 and 14 mm PCs having the most uniform mixture distribution. With a PC throat diameter of 16 mm, a larger volume of low-equivalence ratio mixture flows into the PC from the MC, reducing the overall equivalence ratio of the mixture within the PC.

3.2.2 Main chamber temperature field distribution

Figure 11 illustrates the temperature field distribution in the MC for various throat diameters. At −12° CA aTDC, the high-temperature combustion products from the PC have entered the MC through the orifices and initiated combustion in all six throat diameter scenarios. The PC with a 9 mm throat diameter generates the highest jet flame temperature. A smaller throat diameter results in the formation of a locally overly rich mixture near the spark plug, which increases the energy of the jet flame. At −8° CA aTDC, the MCs with 9, 13, and 14 mm throat diameters exhibit larger high-temperature combustion areas, indicating that combustion begins earlier in these cases than in the three other cases. At 4° CA aTDC, the MC with a 14 mm throat diameter demonstrates the largest flame front area and the most complete combustion. By contrast, the MC with a 16 mm throat diameter shows a smaller flame front area, with a more disordered temperature distribution, where regions of low and high temperatures are intermingled. An overly large throat diameter in the PC causes uneven mixture distribution, leading to incomplete combustion in the MC.

3.2.3 Combustion properties

Figure 12 presents the pressure and HRR curves for the PC. The highest first peak pressure, recorded at 17.8 MPa, occurs in the PC with an 11 mm throat diameter of −12.6° CA aTDC. Slow combustion is observed in PCs with throat diameters of 11, 13, and 16 mm due to uneven mixture distribution. The PC with a 9 mm throat diameter shows the highest HRR, reaching 4.6 kJ at −14.1° CA aTDC. This condition is attributed to the smaller throat diameter, which restricts the entry of low-equivalence ratio mixture from the MC during the piston's upward movement, achieving higher mixture concentration within the PC. As a result, the combustion temperatures and HRR increased, but the risk of knocking in the PC was also elevated. The second half of the HRR curve evidently shows that after the jet phase concludes, some combustion products are forced back into the PC, given that the piston has not yet reached TDC. This effect is most noticeable in PCs with 11- and 16-mm throat diameters.

Figure 13 shows the max pressure difference in the PC for different throat diameters. The earliest occurrence times are for 9, 12, and 14 mm, with maximum pressure differences of 10.2, 9.2, and 10.1 MPa, respectively, correspond-

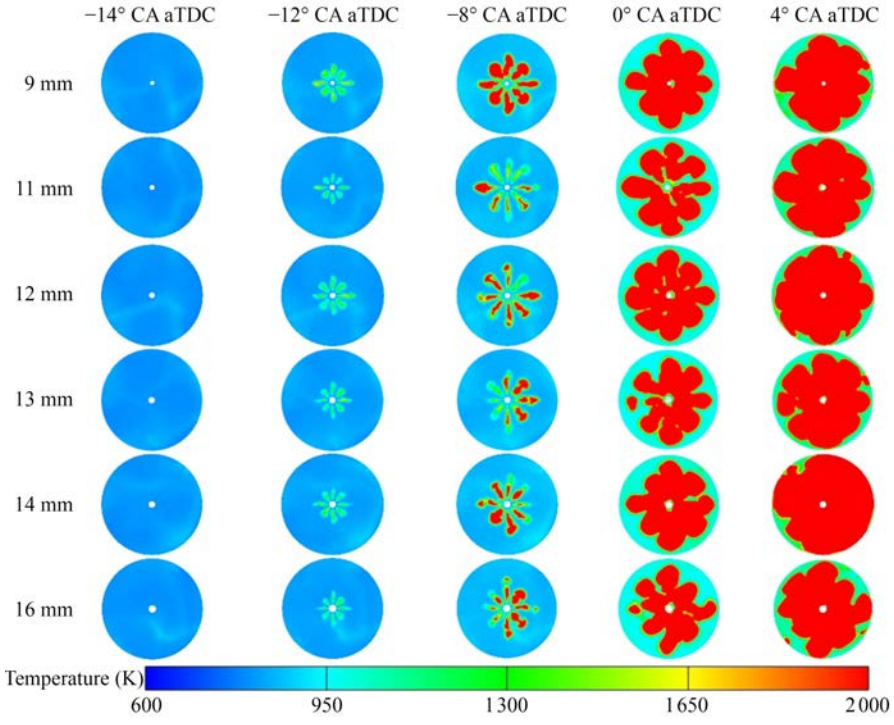

Figure 11 Distribution of temperature field in the MC under different throat diameters

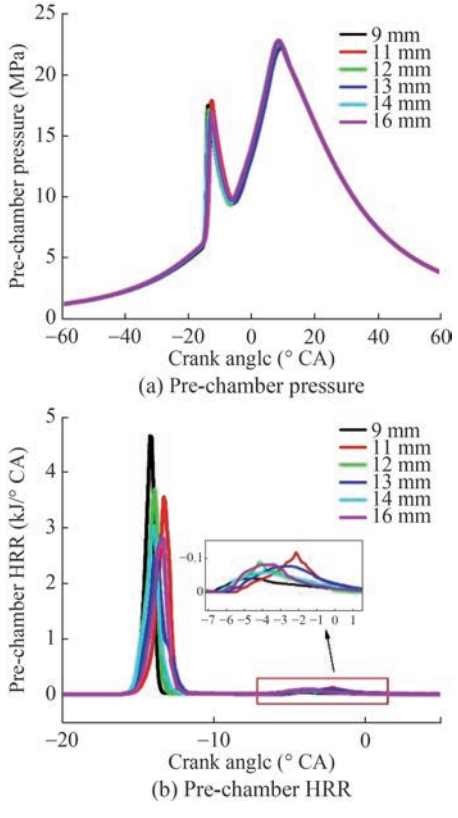

Figure 12 PC pressure and HRR curves under different throat diameters

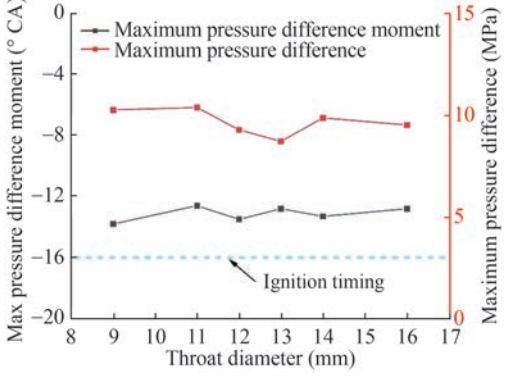

Figure 13 PC pressure difference with different throat diameters

ing to −13.7°, −13.5°, and −13.3° CA aTDC. The throat diameter slightly affects the timing of the max pressure difference in the PC, with the variation across the six cases being less than 1° CA. A higher pressure difference in the PC can produce faster jets, reducing combustion delay in the MC. This finding further explains the differences in jet occurrence times and high-temperature region areas in the temperature field distribution.

Figure 14 illustrates the pressure and HRR curves in the MC. The maximum pressures in the MC for the six cases are 23.2a, 23.3, 23.3, 23.1, 23.4, and 23.3 MPa, occurring at 6.5°, 6.4°, 6.3°, 6.9°, 6.2° and 6.5° CA aTDC, respectively. The max pressures are nearly equal, and the times at which they are reached do not differ significantly. The HRR for the throat diameters of 14 and 16 mm is higher, indicating faster combustion in the cylinder. The HRR for the 12-mm throat diameter is the lowest. Combined with the flame front area size, slower and less complete combustion is observed in the MC. Combustion in the MC is delayed

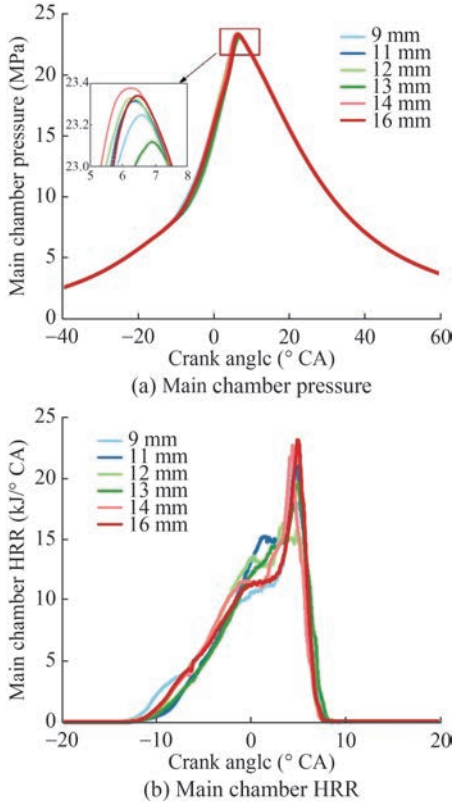

Figure 14 MC pressure and HRR curves under different throat diameters

in four of the cases, with the exception of those with throat diameters of 9 and 14 mm.

Therefore, with constant PC height, altering the throat diameter slightly influences the mixture formation in the PC when the PC volume and the distance between the spark plug and the orifice are fixed. Based on the comparison of the HRR and MC cylinder pressures, the 14 mm throat diameter is selected for further investigation, as it enhances combustion in the MC.

3.3 Distance between hydrogen injector and spark plug

The independent fuel injection system in the active PC plays a crucial role in influencing gas flow. The distance between the hydrogen injector and the spark plug affects the injection location and range of the hydrogen. In this study, the "distance ratio" is defined as the ratio of the distance from the hydrogen injector to the spark plug relative to the PC radius. The analysis of this distance ratio offers valuable insights for designing fuel injection systems in PCs with varying diameters. Considering practical machining issues, the max distance ratio is set to 0.95, ensuring a certain distance between the hydrogen injector and the PC sidewall. As the injected gas creates a flow field upon impacting the PC wall, a distance ratio greater than 0.5 is recommended for optimal performance.

In this study, the distance ratios are set to 0.63, 0.75, 0.84, 0.92, and 0.95, corresponding to hydrogen injector to spark plug distances of 16, 19, 21.5, 23.5, and 24.5 mm, respectively.

3.3.1 Pre-chamber mixture formation

Different distance ratios influence the hydrogen injection location within the PC, leading to variations in the internal flow field. Figure 15 illustrates the velocity vector field and flow distribution inside the PC at the moment of ignition. At this point, the piston presents an upward stroke, and for all distance ratio cases, the highest flow velocity occurs at the throat, whereas the slowest flow is near the PC wall. The flow trajectory reveals a significant vortex formed at the junction between the upper PC region and the throat, creating a more uniform mixture. The average flow speed for the 0.92 distance ratio is higher than that observed in the four other cases. Distinct low-velocity regions are evident in the 0.63 and 0.75 cases because the hydrogen strikes the PC wall sooner when the distance ratio is extremely small, given that the shorter distance between the spark plug and the hydrogen injector reduces the flow speed. As the distance ratio increases, the turbulent area within the PC expands, and the flow speed increases, facilitating improved mixture formation.

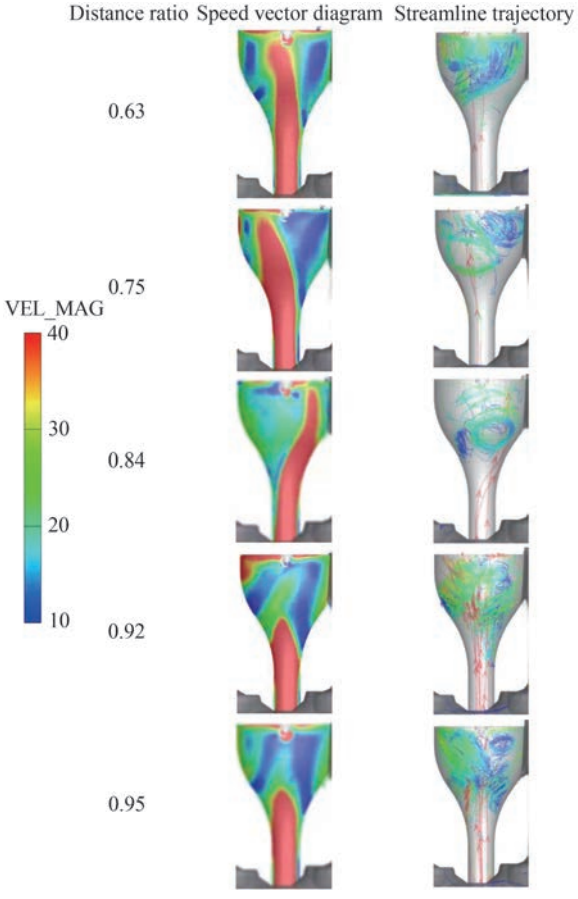

Figure 15 Flow field distribution in the PC at the ignition time

Figure 16 shows the equivalence ratio distribution cloud charts in the PC at ignition timing for different distance ratios. This flow field analysis indicates that the turbulent areas in the 0.63, 0.75, and 0.84 distance ratios are smaller, with lower flow speeds, leading to the formation of uneven, locally overly lean mixtures. The turbulent areas in the 0.92 and 0.95 distance ratios are larger, resulting in a homogeneous mixture.

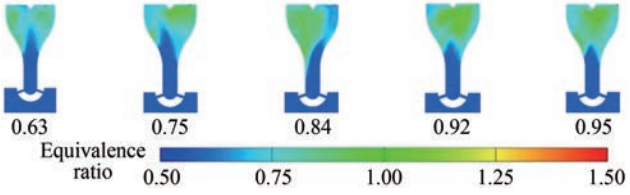

Figure 16 Distribution cloud diagram of PC equivalence ratio at ignition time

3.3.2 Temperature field distribution in pre-chamber and main chamber

Figure 17 illustrates the temperature field distribution in the PC and MC for various distance ratios. At −14° CA aTDC, the combustion rates in the PC are slower for distance ratios of 0.63 and 0.84, with high-temperature regions concentrated around the spark plug. By contrast, for distance ratios of 0.75, 0.92, and 0.95, combustion occurs more rapidly, with flames spreading toward the throat of the PC. At −12° CA aTDC, the jet flames for all cases have reached the MC and started burning. The jet flames for 0.92 and 0.95 are uniformly distributed, with approximately the same temperature for each jet, while those for 0.63 and 0.75 exhibit uneven distribution, with varying temperatures for each jet. At −8° CA aTDC, the high-temperature region of the jet flame for 0.92 is the largest, facilitating rapid ignition of the MC mixture. At 4° CA aTDC, the flame front area is still the largest for 0.92, and the MC does not exhibit interwoven high- and low-temperature regions, indicating MC complete combustion.

3.3.3 Combustion properties

Tumble and swirl ratios are used to measure the motion of in-cylinder gases. In a gas-fueled engine, the motion state of the PC mixture significantly impacts engine combustion and performance. The tumble ratio is the ratio of the rotational speed of the tumbling mixture to the engine's speed. A higher tumble ratio signifies greater kinetic energy in the in-cylinder flow, promoting more uniform mixture distribution and resulting in more efficient combustion.

Figure 18 presents a comparison of the tumble and swirl ratios for different distance ratios at ignition timing. The smallest tumble and swirl ratios are for the 0.75 distance ratio, with values of 0.08 and 0.88, respectively. When the

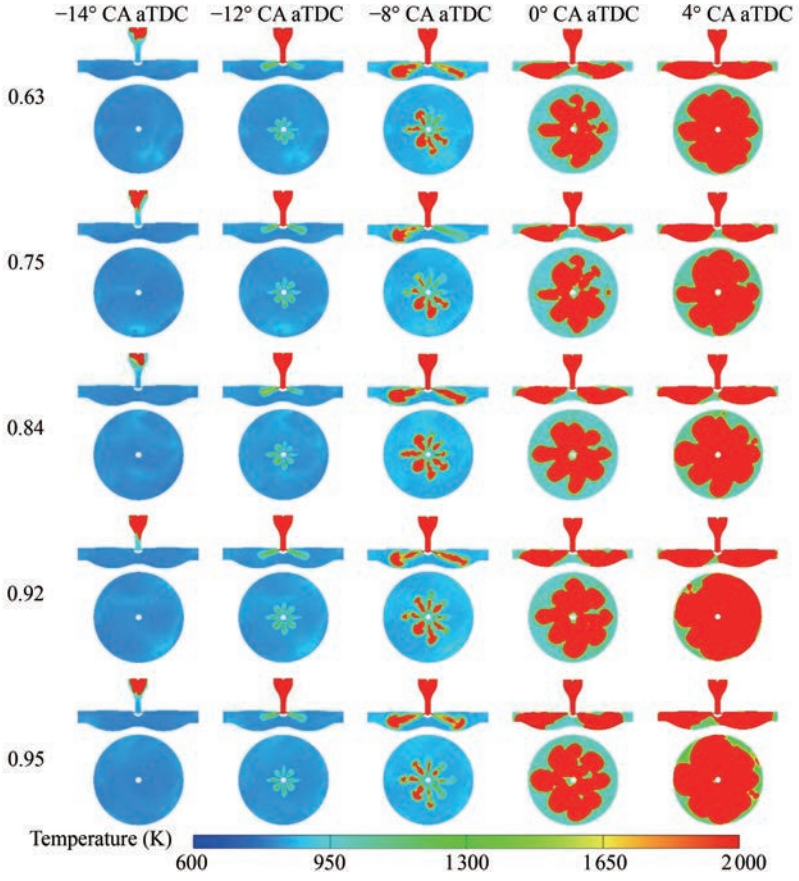

Figure 17 Temperature distribution of PC and MC at different distance ratios

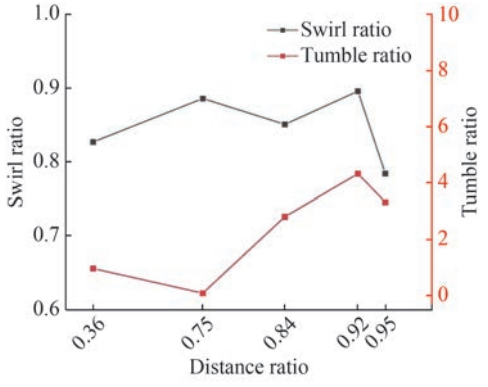

Figure 18 Tumble and swirl ratios of the PC at different distance ratios

hydrogen injector is close to the spark plug, the injection position of hydrogen is in the middle of the PC, causing difficulty in forming strong tumbling. The 0.92 distance ratio has the highest tumble and swirl ratios, at 4.32 and 0.89, respectively, with the tumble ratio being tens of times greater than that of the 0.75 ratio. A larger distance ratio allows hydrogen to flow along the sidewall of the PC, forming high-intensity tumbling.

Figure 19 illustrates the variation of turbulent kinetic energy (TKE) in the pre-chamber under different distance ratio cases. The figure suggests that the TKE in the pre-chamber begins to increase from −121° CA. At this point, hydrogen is injected into the pre-chamber through the hydrogen injector, causing changes in the flow field. As the piston continues to increase, the mixture from the MC is pushed into the pre-chamber, causing the TKE in the pre-chamber to continuously increase. At the moment of ignition, a peak in TKE is observed in the pre-chamber. Subsequently, as the mixture in the pre-chamber forms a jet flame and enters the MC, the TKE decreases. At approximately 10° CA, the TKE in the pre-chamber reaches its maximum value of 0.92, indicating that combustion in the MC is complete, generating higher pressure and causing more significant changes in the flow field of the pre-chamber.

As depicted in Figure 20, the highest first peak pressure in the PC occurs with a distance ratio of 0.95, reaching

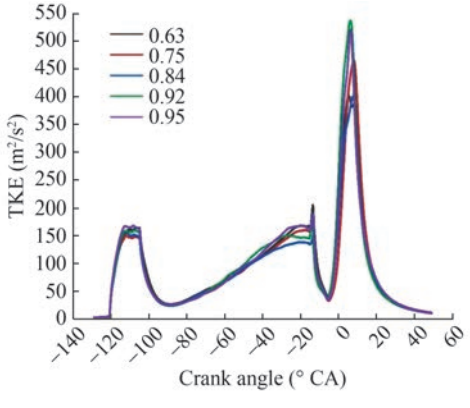

Figure 19 TKE of the PC at different distance ratios

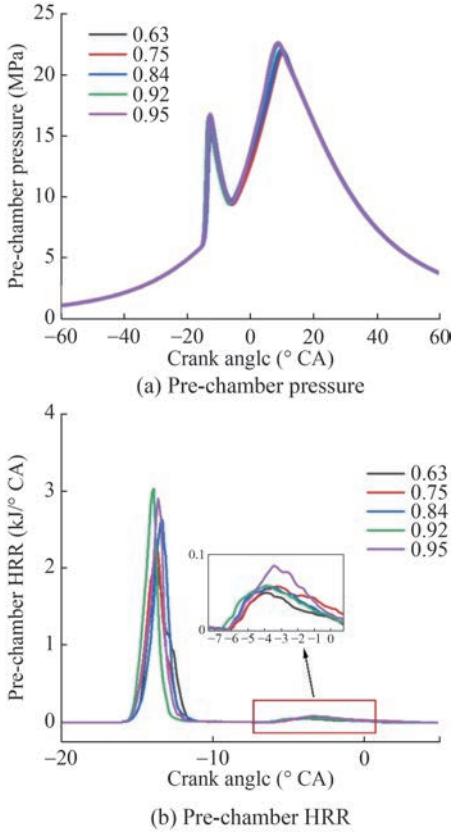

Figure 20 PC pressure and HRR curves under different distance ratios

16.7 MPa at −12.8° CA. The first peak pressures for ratios of 0.84 and 0.92 are similar at 16.5 MPa, occurring at −12.6° and −13.1° CA, respectively. The former reaches peak pressure later, indicating slower PC combustion. The HRR for 0.92 is the highest, reaching 3.1 kJ at −13.9° CA. The HRR increases sequentially from 0.63 to 0.84, with the peak HRR for 0.84 occurring at −13.3° CA, indicating the slowest PC combustion. Before reaching TDC, the 0.95 distance ratio presents a significant diffusion of combustion products from the MC into the PC, indicating the most intense combustion in the MC.

A higher first peak pressure in the PC generates a higher energy jet, leading to faster combustion in the MC. As illustrated in Figure 21, the MC pressure for the distance ratio of 0.95 is the highest, with a peak pressure of 23.6 MPa at 5.7° CA. The peak pressures for the four other cases are 23.4, 22.7, 22.6, and 22.4 MPa, occurring at 6.1°, 7.7°, 8.0°, and 8.4° CA, respectively. As the distance ratio decreases, the peak pressure in the MC decreases, and the combustion speed gradually decreases. The highest HRR is achieved for 0.95, reaching 27.6 kJ at 4.6° CA. The peak HRR for 0.63, 0.75, and 0.84 does not exceed 20 kJ. The peak HRR for 0.92 and 0.95 has reached 4.4° and 4.6° CA, respectively, whereas the three other cases exhibit combustion delay.

Increasing the distance ratio promotes the formation of tumble in the PC, leading to a more homogeneous mixture,

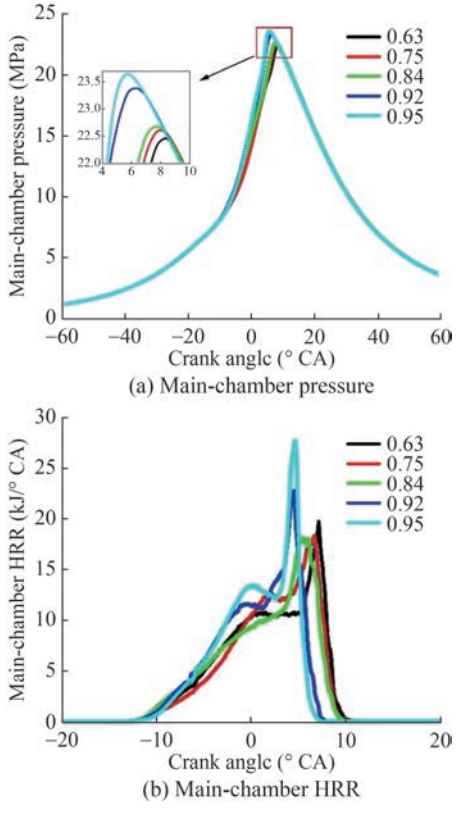

Figure 21 MC pressure and HRR curves under different distance ratios

faster PC combustion speed, and higher energy jet flames, thereby improving combustion in the MC. However, an excessively large distance ratio is not conducive to machining and installation. A larger distance ratio within a reasonable range can be selected for the PC. A PC with a distance ratio of 0.92, corresponding to a hydrogen injector to spark plug distance of 23.5 mm, is selected for further research.

3.4 Angle of hydrogen injector in pre-chamber

The fuel injection angle in the PC is another crucial factor influencing the formation of the mixture within the PC. Varying flow directions results in different types of flow patterns and levels of TKE inside the PC. In this study, hydrogen is injected into the PC, and the mixing efficiency of the gaseous fuel becomes more susceptible to the internal flow field dynamics within the PC. This section selects an angle range of 50°–90°, with each 10° interval considered a case, namely D50, D60, D70, D80, and D90.

3.4.1 Pre-chamber mixture formation

Figure 22 illustrates the distribution of the velocity vector field and streamlines in the PC at ignition timing. In the upper section of the PC, D50, D70, and D90 exhibit the fastest flow speeds along the throat diameter, whereas D60 and D80 form more evenly distributed flow fields. In D50, a noticeable small vortex forms between the upper region of the PC and the throat. D70 presents a large area

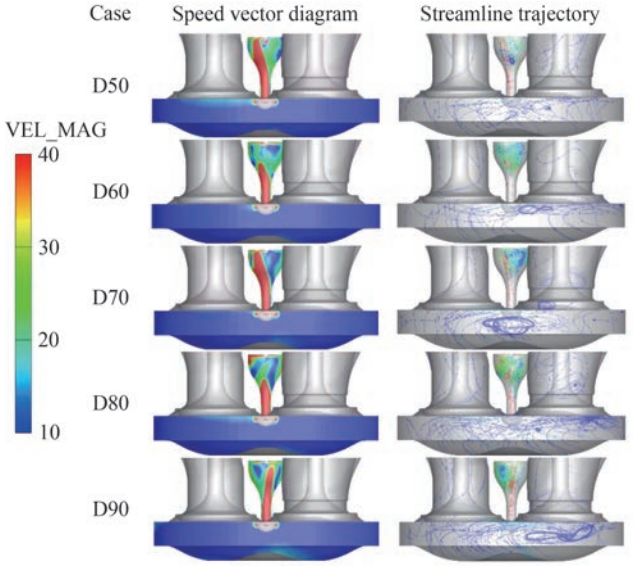

Figure 22 Flow field distribution in the PC at different hydrogen injector angles

of excessively slow flow speeds because the injection angle points toward the PC throat, slowing the flow speed in the upper segment of the PC. D80 forms the largest turbulent flow field area, which is beneficial for homogeneous mixture formation.

The flow fields formed by D70 and D90 are on one side of the PC, failing to create a centrally located flow field. When the hydrogen injector angle is extremely small, the direction of hydrogen movement does not follow the PC wall, preventing the formation of high-intensity tumbling. When the angle is extremely large, collisions between the hydrogen and PC wall increase kinetic energy loss, thereby reducing mixture flow speed.

As illustrated in Figure 23, the mixture formed in D80 exhibits an equivalence ratio closest to 1, whereas the four other cases exhibit locally overly lean distributions. During the piston's upward stroke, when an excessive amount of the lean mixture enters the PC, localized regions demonstrate overly lean mixture distributions. A stable and large turbulent flow field can promote the formation of a homogeneous PC mixture.

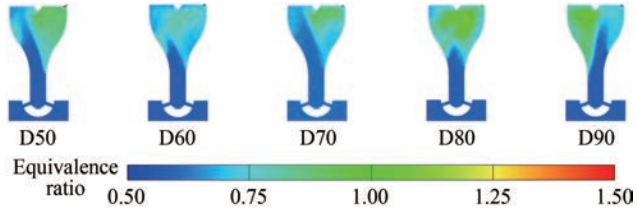

Figure 23 Distribution of PC equivalence ratio at different hydrogen injector angles

3.4.2 Pre-chamber temperature field distribution

Figure 24 presents the temperature field distribution in the PC for various hydrogen injector angles, illustrating the

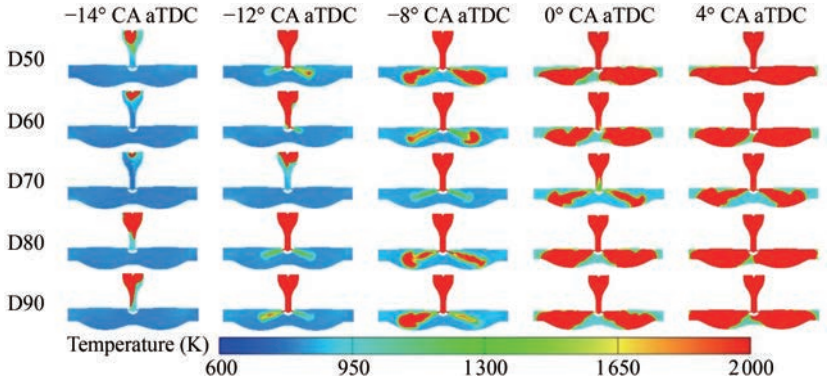

Figure 24 Distribution of PC temperature field at different hydrogen injector angles

formation and progression of jet flames. At −12° CA aTDC, D50, D80, and D90 have already produced jet flames, whereas the flame in D60 has just reached the PC orifice. The combustion in the D70 PC is noticeably delayed. At −8° CA aTDC, the jet flame distribution in D80 is uniform, with a slight difference in single-hole jet flow rate and temperature, thereby promoting complete combustion in the MC. At 4° CA aTDC, the high-temperature region formed by D80 almost encompasses the entire MC. A well-combined homogeneous mixture promotes the development of jet flames, enhances flame propagation speed, accelerates combustion in the MC, and reduces the ignition delay period within the MC.

3.4.3 Combustion properties

As shown in Figure 25, the tumble ratio for D80 is the highest at 4.3, whereas the tumble ratio for D70 is the lowest at 0.07. The strong tumbling generated by D80 creates a more homogeneous mixture, which in turn enhances the combustion speed and flame propagation within the PC. The swirl ratio for D50 is the lowest at 0.2, whereas the swirl ratios for D60, D70, D80, and D90 are 0.73, 0.79, 0.89, and 87, respectively. Variations in the hydrogen injector angle slightly affect the PC swirl formation.

Figure 26 illustrates the PC pressure and HRR curves. The highest first peak pressure in the PC is for D50, with a value of 16.58 MPa at −12.8° CA. The first peak pressure for D80 is 16.56 MPa, occurring at −13.2° CA. The peak pressures of D50 and D80 differ by only 1.2%, but D50 exhibits slow combustion. The first peak PC pressure for D70 is the lowest, occurring at −10.1° CA, indicating the slowest combustion. The first to reach the peak HRR is D90, with a value of 3.1 kJ at −14.1° CA. The peak HRR values for the other cases are 2.9, 1.8, 1.1, and 3.03 kJ, occurring at −12.4°, −11.6°, −13.8°, and −13.9° CA, respectively. The peak HRR values for D80 and D90 are relatively high, with faster combustion. As a result of the uneven mixture distribution, D70 obtains the lowest peak HRR and first peak pressure.

As illustrated in Figure 27, the pressure in the MC does not exhibit a consistent monotonic trend. The tumble ratio

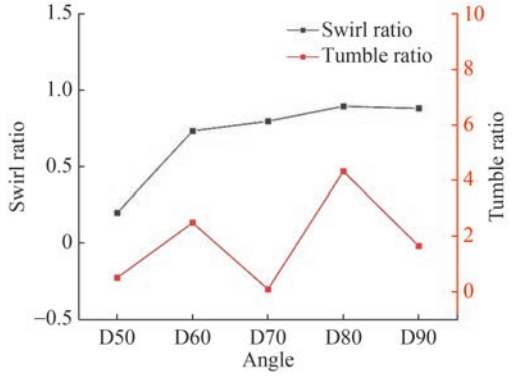

Figure 25 Tumble and swirl ratios of the PC at different hydrogen injector angles

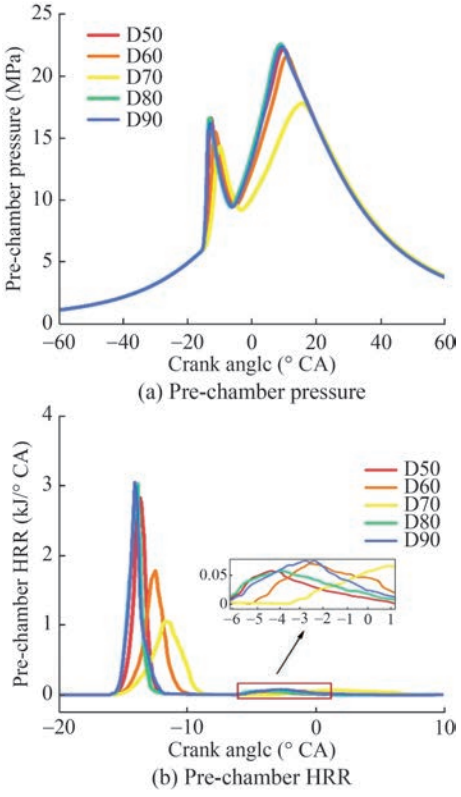

Figure 26 PC pressure and HRR curves under different hydrogen injector angles

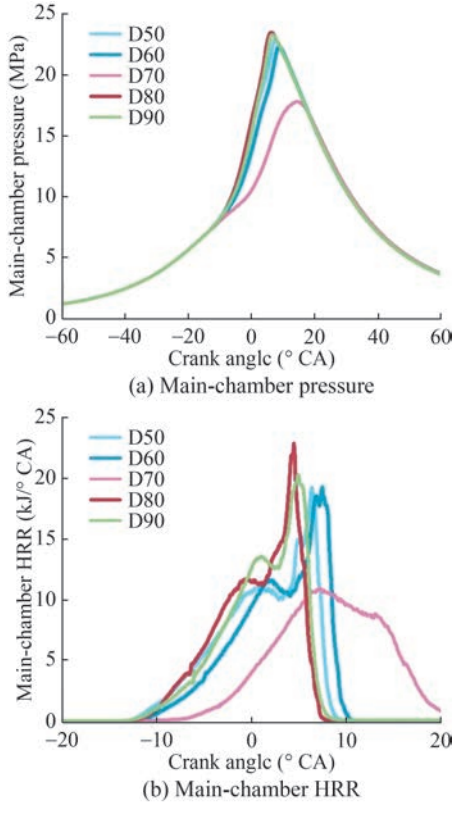

Figure 27 MC pressure and HRR curves under different hydrogen injector angles

of the mixture in the PC is influenced by different injection angles, with excessively large and small angles that reduce the tumble ratio. The max MC peak pressure is 23.4 MPa, occurring at 6.1° CA, with the hydrogen injection angle at 80°. The peak pressures in the MC from highest to lowest are 23.2, 22.8, 22.2, and 17.7 MPa, corresponding to D90, D50, D60, and D70, respectively. The corresponding times for the peak pressures are progressively delayed at 6.5°, 7.6°, 8.8°, and 14.2° CA. Combustion in the MC is significantly slower for D60 and D70.

4 Conclusions

This study has investigated the impact of PC design parameters, including throat diameter, distance ratio, and hydrogen injector angle, on the combustion characteristics of PCI. The following conclusions can be drawn using the analysis:

1) Variations in the PC throat diameter affect the flow velocity and combustion efficiency. A throat diameter of 14 mm was found to strike the best balance, achieving optimal jet velocity and combustion efficiency. On the contrary, excessively large or small diameters led to lower performance due to uneven mixture distribution and slower flame propagation.

2) The distance ratio, the ratio between the hydrogen injector and the spark plug relative to the PC radius, also considerably influences combustion. A higher distance ratio, such as 0.92, promotes a more homogeneous mixture formation, faster combustion, and improved flame propagation in the MC. Smaller distance ratios, on the contrary, resulted in slower flow speeds and less effective mixing.

3) The angle of hydrogen injection plays a crucial role in the flow dynamics within the PC. Larger injection angles facilitate enhanced mixture formation, but excessively large or small angles can reduce the tumble ratio, impacting the overall combustion process. An optimal range of injection angles maintains a balanced tumble ratio, leading to more efficient combustion.

4) The study demonstrates that an appropriate combination of throat diameter, distance ratio, and injection angle can significantly enhance combustion performance by promoting faster flame propagation and more uniform mixture distribution. The PC with a 14 mm throat diameter and a 0.92 distance ratio exhibited the best overall performance, with improved combustion speed, higher peak pressures, and complete combustion. The first peak pressure in the PC is 16.56 MPa, with a maximum HRR of 3.03 kJ/° CA. The peak pressure in the MC is 23.4 MPa, with a maximum HRR of 22.7 kJ/° CA. The performance of the original engine is significantly improved by altering its fuel and PC structure. The peak pressure in the PC is increased by 23.1%, and that in the MC is increased by 46.3%.

5) Further experimental studies are required to validate the numerical findings and optimize the PC design for different fuel types and operating conditions. Investigating the effects of varying fuel compositions, such as ammonia-hydrogen mixtures, under different PC configurations would provide deeper insights into enhancing combustion efficiency.

Funding Supported by the Priority Academic Program Development of Jiangsu Higher Education Institutions under Grant No. 014000319/2018-00391.

Competing interest The authors have no competing interests to declare that are relevant to the content of this article.

References

Anderson A, Chen TN, Hutchins WT (1984) The development and application of design criteria for pre-combustion chambers on natural gas fueled engines. Mechanical Engineering 106(5): 94

Attard WP, Fraser N, Parsons P, Toulson E (2010) A turbulent jet ignition pre-chamber combustion system for large fuel economy improvements in a modern vehicle powertrain. SAE Technology Paper 3(2): 20-37. https://doi.org/10.4271/2010-01-1457

Biswas S, Qiao Li (2018) Ignition of ultra-lean premixed H2/air using multiple hot turbulent jets generated by pre-chamber combustion. Applied Thermal Engineering 132: 102-114. https://

doi.org/10.1016/j. applthermaleng.2017.11.073

Bunce M, Blaxill H, Kulatilaka W, Jiang NB (2014) The effects of turbulent jet characteristics on engine performance using a pre-chamber combustor. SAE Technical Paper 01: 1195. https://doi.org/10.1002/abio.370040210

Dale J, Oppenheim A (1981) Enhanced ignition for I. C. engines with premixed gases. SAE Trans 810146: 606-621. https://doi.org/10.1002/abio.370040210

Haruna A, Tanimu G, Ibrahim I, Garba ZN, Yahaya SM, Musa SG, Merican ZMA (2023) Mitigating oil and gas pollutants for a sustainable environment–Critical review and prospects. Journal of Cleaner Production 416: 137863. https://doi.org/10.1016/j.jclepro.2023.137863

Hlaing P, Marquez ME, Cenker E, Im HG, Johansson B, Turner JWG (2022) Effects of volume and nozzle area in narrow-throat spark-ignited pre-chamber combustion engines. Fuel 313: 123029. https://doi.org/10.1016/j.fuel.2021.123029

Jamrozik A (2015) Lean combustion by a pre-chamber charge stratification in a stationary spark ignited engine. J. Mech. Sci. Technol. 29(5): 2269-2278. https://doi.org/10.1007/s12206-015-0145-7

Kleeman MJ, Zapata C, Stilley J, Hixson M (2013) PM2.5 co-benefits of climate change legislation part 2: California governor's executive order S-3-05 applied to the transportation sector. Nature Climate Change 117(1-2): 399-414. https://doi.org/10.1007/s10584-012-0546-x

Latsch R, Schlembach H (1980) Externally ignited internal combustion engine. US Patent 4 218: 992

Liu XL, Aljabri H, Panthi N, AlRamadan AS, Cenker E, Alshammari AT, Magnotti G, Im HG (2023a) Computational study of hydrogen engine combustion strategies: Dual-Fuel compression ignition with Port- and Direct-Injection, Pre-Chamber Combustion, and Spark-Ignition. Fuel 350: 128801. https://doi.org/10.1016/j.fuel.2023.128801

Liu Z, Zhou L (2023) Enhanced combustion of ammonia engine based on novel air-assisted pre-chamber turbulent jet ignition. Energy Convers Manag 276: 116526. https://doi.org/10.1016/j.enconman.2022.116526

Liu Zongkuan, Wei Haiqiao, Shu Gequn, Zhou Lei (2023b) Ammonia-hydrogen engine with reactivity-controlled turbulent jet ignition. Fuel 348: 128580. https://doi.org/10.1016/j.fuel.2023.128580

Liu Zongkuan, Zhou Lei, Zhong Lijia, Liu Peilin (2022) Experimental investigation on the combustion characteristics of NH3/H2/air by the spark ignition and turbulent jet ignition. Combustion Science and Technology 196(1): 73-94. https://doi.org/10.1080/00102202.2022.2063687

Sun X, Liu H, Duan X, Guo H, Li Y, Qiao J, Liu Q, Liu J (2022) Effect of hydrogen enrichment on the flame propagation, emissions formation and energy balance of the natural gas spark ignition engine. Fuel 307: 121843. https://doi.org/10.1016/j.fuel.2021.121843

Validi A, Schock H, Jaberi F (2017) Turbulent jet ignition assisted combustion in a rapid compression machine. Combustion and Flame 186: 65-82. https://doi.org/10.1016/j.combustflame.2017.07.032

Wu H, Wang L, Wang X, Sun B, Zhao Z, Lee CF, Liu FS (2018) The effect of turbulent jet induced by pre-chamber sparkplug on combustion characteristics of hydrogen-air pre-mixture. Int J Hydrogen Energy 43: 8116-26. https://doi.org/10.1016/j.ijhydene.2018.02.155

Yu Zhiqing, Li Xiang, Zhao Jianhui, Shi Lei (2024) Development of ammonia reaction kinetic mechanism under engine-relevant conditions. Energy & Fuels 38(1): 728-741. https://doi.org/10.1021/acs.energyfuels.3c03241

Zhu Sipeng, Akehurst S, Lewis A, Yuan H (2022) A review of the pre-chamber ignition system applied on future low-carbon spark ignition engines. Renewable and Sustainable Energy Reviews 154: 111872. https://doi.org/10.1016/j.rser.2021.111872